Oxide Sandwiched Metal Thin-Film Electrodes for Long-Term Stable Organic Solar Cells

Sylvio Schubert, Martin Hermenau, Jan Meiss, Lars Müller-Meskamp,* and Karl Leo*

Oxide/silver/oxide multilayers as semitransparent top electrode for small molecule organic solar cells (OSCs) are presented. It is shown that two oxide layers sandwiching a central metal layer greatly improve the stability and lifetime of the organic solar cell. Thermally evaporated MoO_3, WO_3, or V_2O_5 layers are employed as an interlayer for subsequent silver deposition and significantly change the morphology of the ultrathin silver layer, improving charge extraction and electrodes series resistance. The transmittance of the electrode is increased by introducing oxide or oxide and organic multilayers as capping layer, which leads to higher photocurrent generation in the absorber layer. Application of 1 nm MoO_3/11 nm Ag/10 nm MoO_3/50 nm Alq_3 multilayer electrodes in OSCs lead to an efficiency of 2.6% for a standard ZnPc:C60 cell, showing superior performance compared to devices with pure silver top contacts. The device lifetime is also strongly increased. MoO_3 layers can saturate and stabilize the inner and outer metal surface, passivating it against most of the degradation mechanisms. With such an oxide/silver/oxide multilayer electrode, the time until the glass encapsulated OSC is degraded to 80% of its starting efficiency is enhanced from 86 h to approximately 4500 h compared to an OSC without an oxide interlayer.

1. Introduction

Since Tang published an organic heterojunction solar cell (OSC) in 1986,[1] continuous advancements in material and concept development have led to great device improvements with certified OSC efficiencies increasing to up to 10.0%[2] and first products having entered the market. Other organic electronic devices like organic light emitting diodes[3] or organic field effect transistors[4] are being broadly investigated and offer attractive properties for novel applications.

Currently indium tin oxide (ITO) sputtered on glass is the standard electrode for OSCs, providing excellent properties in light transmission and electrical conductivity. However, organic materials offer the potential for cheap roll-to-roll manufacturing of flexible and light-weight devices by using flexible substrates and electrodes. For OSCs fabricated on e.g. opaque metal foil or for semitransparent OSCs, a device architecture with semitransparent top contact is required. Since ITO and similar transparent conductive oxides are brittle[5] and the standard sputtering processes could destroy underlying organic molecules, an alternative top contact is necessary. For small molecule OSCs, conductive polymers[6] or silver nanowires[7] are successfully employed as transparent bottom-electrodes, but suffer from the negative effects of solvents on organic materials when applied as top-electrodes. Preparation and deposition of carbon nanotubes or graphene[8] on top of the device is expensive and difficult without breaking the vacuum. In contrast, semitransparent thin metals (<20 nm) in a dielectric/metal/dielectric configuration, which are used in this paper exhibit high conductivities and transparencies.[9] Transition metal oxides can be used as dielectric materials and are thermally evaporable in vacuum "in-line" like all other layers of a small molecule OSC. They are already successfully employed as part of the electrode or hole transport layer in OSCs.[10–12] Here we focus on the application of metal oxides as template for silver deposition and investigate its influence on the device stability.

The thermally evaporated metal layers on transition metal oxides investigated here, experience Volmer-Weber growth, which starts from disconnected nuclei.[13] Thus, due to the clustering for very thin layers, the optical and electrical properties are often unfavorable, and it is critical to control the growth process. After further deposition the percolation threshold is reached, which is defined as equivalent thickness where separate metal islands start to connect and form a continuous layer. The regime showing the best trade-off between increasing conductivity and decreasing transparency is close to this transition point. The percolation threshold thickness strongly depends on metal type, substrate, temperature, or surfactants.[13–16] Furthermore, the small process window for application makes the thin metal electrode very susceptible for degradation.[17–19] Here we report on thin silver electrodes for OSCs grown on various transition metal oxides like MoO_3, WO_3, and V_2O_5 which are then subsequently covered by MoO_3 resulting in stable and more efficient devices.

S. Schubert, M. Hermenau, Dr. J. Meiss,[+]
Dr. L. Müller-Meskamp, Prof. K. Leo
Institut für Angewandte Photophysik
Technische Universität Dresden
George-Bähr Straße 1, 01062 Dresden, Germany
E-mail: sylvio.schubert@iapp.de;
lars.mueller-meskamp@iapp.de
[+] Present address: Reiner Lemoine Institut gGmbh, Ostendstraße 25, 12459 Berlin, Germany

DOI: 10.1002/adfm.201201592

© 2012 WILEY-VCH Verlag GmbH & Co. KGaA, Weinheim

2. Results and Discussion

In this paper, we present OSC with oxide/silver/oxide top electrodes. All materials are deposited by thermal evaporation in vacuum. Thus, this kind of electrode is a promising candidate for cost efficient and fast mass production. Still, the thermal evaporation of metal oxides is challenging because most of them sublime at very high temperatures or dissociate. As a first step we try to evaporate the metal oxides MoO_3, WO_3, V_2O_5, GeO_2, and Cu_2O on glass and measure their surface roughness, optical transparency, and conductivity (the complete set of information can be found in the Supporting Information Figure S1,S2). The experiments show that Cu_2O dissociates in our setup, resulting in very high chamber pressure (>10^{-4} mbar, compared to the base pressure of 10^{-8} mbar) and only opaque, metallic Cu is deposited. GeO_2 is deposited as transparent oxide but the chamber pressure is again too high for reliable device fabrication. In contrast, thermal evaporation of MoO_3, WO_3, and V_2O_5 works well and no significant increase in pressure is observed. 50 nm thin layers of these three oxides show high transparencies of 73%, 76%, and 69%, respectively, at a wavelength of 600 nm, high sheet resistances of 160, 740 and 1.5 $G\Omega_{sq}$ and a very smooth surface with a root mean square roughness lower than 0.22 nm on a $5 \times 5\ \mu m^2$ area, measured by AFM.

The oxides are applied at two positions in the OSC stack. First, as interlayer between organic layers and thin silver electrode and second, as capping layer (see **Figure 1**). Both applications are investigated separately. Note that the high resistivity limits the interlayer thickness. We find an 4 nm oxide is thin enough to efficiently transport charge carriers to the electrode and also thick enough to form a closed layer.

Figure 2 shows the current density vs. voltage plot of four identical OSCs under illumination, using 14 nm silver with and without different oxide interlayers as semitransparent top electrode. The corresponding solar cell characteristics are summarized in **Table 1** as well as series (R_{series}) and shunt resistances (R_{shunt}). Since the open circuit voltage (V_{OC}) is determined by the energy levels of the absorber materials, it remains constant at 0.52 V when the interlayer is varied. A significant "S-kink",[20] low fill factor (*FF*) and therefore lowest power conversion efficiency (η = 1.5%) of the sample without an interlayer hint at issues in charge extraction, or high recombination. This can be caused by the silver layer, which interacts with or diffuses into the organic sublayer.[21] Additionally the thin silver forms disconnected islands trapping charge carriers, which leads to an increased series resistance. In contrast, the samples with oxide interlayer do not show this "S-kink" resulting in a strong increase in efficiency up to 2.0% by using MoO_3. The slope of the current density in forward direction is much higher for the samples with MoO_3 interlayer, implying an improved hole collection and lower series resistance. However, the short circuit current density (J_{SC}) is smaller for samples which contain WO_3 (6.82 mA/cm^2) or V_2O_5 (6.62 mA/cm^2) compared to 7.42 mA/cm^2 using no oxide interlayer. Only the OSC with MoO_3 interlayer shows a superior J_{SC} of 7.54 mA/cm^2. These differences in J_{SC} are attributed to different morphologies of the thin silver electrode and therefore different transparencies in agreement with the measurements discussed below.

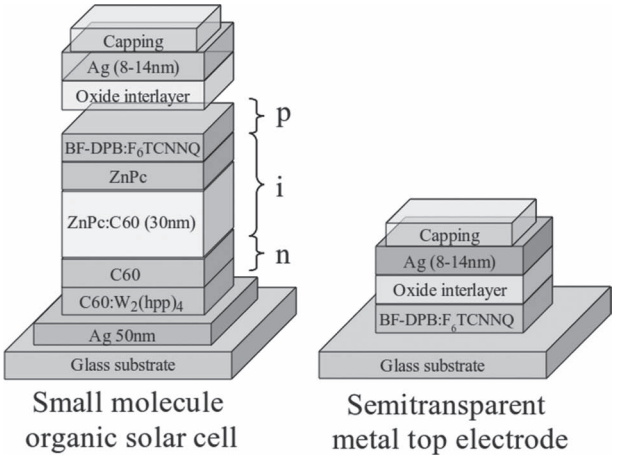

Figure 1. Stack design of small molecule organic solar cell and top-electrode-only samples. The top-electrode-only samples are used to study conductivity and optical properties. Top illumination from the capping layer side is applied for characterization of both sample types.

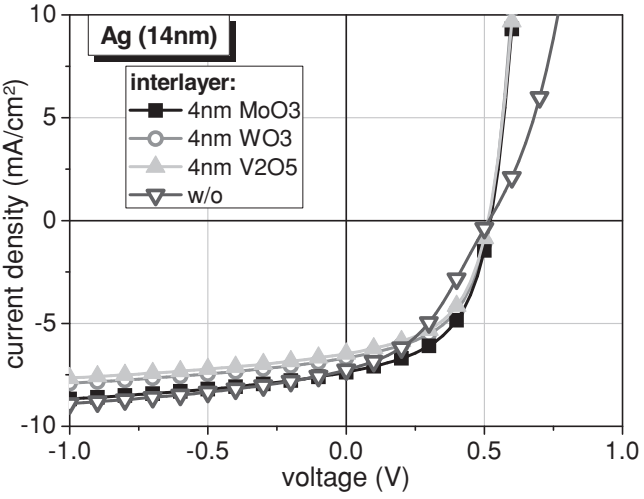

Figure 2. Current density–voltage curves of OSCs with 14 nm Ag electrodes and different oxide interlayers, under illumination (simulated AM 1.5G, 100 mW/cm^2). The interlayer is varied with 4 nm MoO_3 (squares), 4 nm WO_3 (empty circles), 4 nm V_2O_5 (up triangles), or without (empty down triangles). No capping is used.

Table 1. Solar cell characteristics depending on the interlayer, obtained under illumination with a light intensity of 100 mW/cm^2. No capping is used. For each interlayer, four identical samples are produced and efficiency deviations are stated.

interlayer	V_{OC} [V]	J_{SC} [mA/cm^2]	*FF* [%]	η [%]	R_{series} [Ω]	R_{shunt} [Ω]
4 nm MoO_3	0.52	7.54	51.3	1.96 ± 0.06	35	12820
4 nm WO_3	0.52	6.82	51.9	1.82 ± 0.01	39	12180
4 nm V_2O_5	0.51	6.62	51.4	1.70 ± 0.03	79	13180
without	0.52	7.42	39.7	1.45 ± 0.07	113	9810

© 2012 WILEY-VCH Verlag GmbH & Co. KGaA, Weinheim

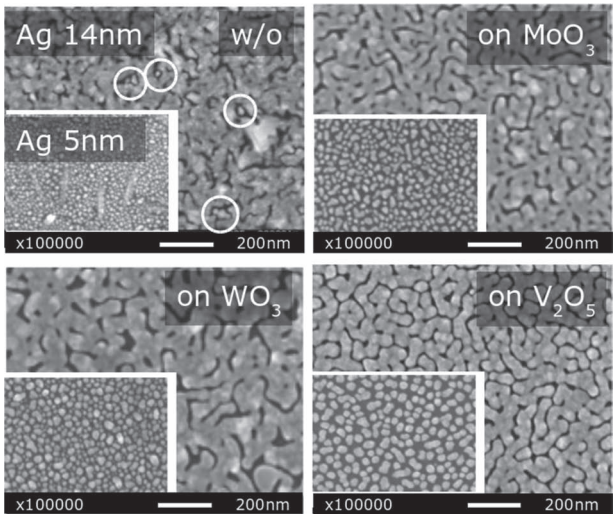

Figure 3. SEM images of solar cell stacks with 5 nm or 14 nm Ag top contact layers on different interlayer. The white scale bar represents 200 nm. The circles highlight examples of isolated clusters. With oxide interlayer the nuclei density is reduced and the surface roughness is increased.

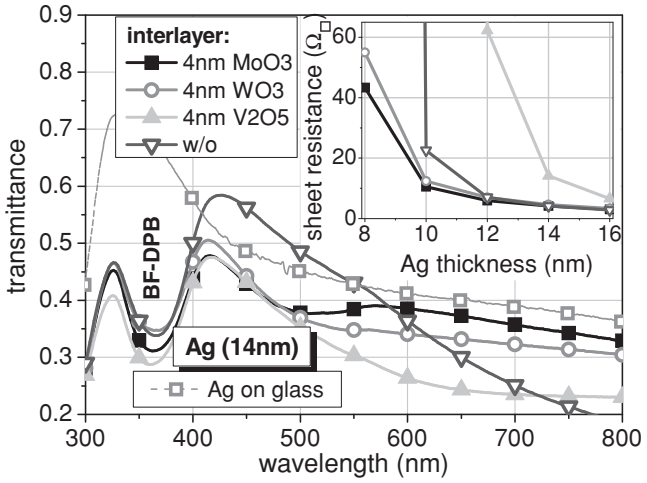

Figure 4. Transmittance of 14 nm thick Ag electrodes deposited on BF-DPB and glass substrate with 4 nm MoO_3 (squares), 4 nm WO_3 (empty circles), 4 nm V_2O_5 (up triangles), or without (empty down triangles) interlayer. For comparison a sample with Ag directly deposited on glass (empty squares) is depicted. The inset depicts the electrode's sheet resistance over Ag layer thickness. The interlayer-dependent morphology of the Ag layer causes significant deviations in transmittance and conductance of the electrode.

In **Figure 3** scanning electron microscopy (SEM) images of the 14 nm thick silver electrode on top of the complete OSC are shown. Different interlayers of the better performing oxides (MoO_3, WO_3, V_2O_5) are studied. The insets show identical samples with the respective interlayers but 5 nm Ag thickness to illustrate the growth of the silver layer, the full image shows the surface after 14nm of silver deposition. The silver layer, which is deposited directly on the organic hole transport layer (BF-DPB) grows with high nucleus density. At 5 nm Ag thickness there are still surface clusters of organic molecules visible (elongated bright structures). This confirms the assumption of silver interaction with the organic material. At 14 nm Ag thickness the layer is still not completely closed, many long, tortuous cracks and isolated regions are visible which can explain the lower current in forward direction. The electrode morphology is drastically changed by introducing oxide interlayers. The interaction of silver with the organic underlayer seems to vanish which is the reason for the improved *FF* (from 39.7% without oxide up to 51.9% with oxide interlayer). Still, the wetting behavior of silver on the oxide surface is not perfect. This leads to an enhanced silver diffusion on the oxide surface compared to the diffusion on the organic layer, resulting in a lower number of nuclei and more evolved nanostructures with high surface roughness. Large uncovered areas are visible at 5 nm Ag thickness. Silver on MoO_3 shows the best wetting and silver on V_2O_5 the worst. The high surface roughness (which is also present for 14 nm silver thickness) causes strong surface plasmon resonances in the visible spectral range.[22,23] These resonances lead to increased light absorption in the electrode and therefore lower generation of photocurrent. **Figure 4** shows the wavelength dependent transmittance of 14 nm thin silver layers on varying oxide interlayers equivalent to those used for the solar cells in Figure 2. At 360 nm the absorption band of the organic layer BF-DPB is visible. From 400 nm to 600 nm the transmittance of the sample without an oxide interlayer is the highest. For silver grown on oxide, the transmittance is generally decreased, which is attributed to morphology related losses. The MoO_3 sample with the lowest surface roughness shows the highest transmittance, particular at longer wavelengths. The V_2O_5 sample with the highest roughness exhibits the lowest transmittance. Between 600 nm and 800 nm, where the light absorption in the photo-active layer is most efficient, the transmittance can be improved with a MoO_3 interlayer. The line with open squares shows Ag deposited directly on glass. Again, the spectrum is strongly changed pointing out the surface dependency of optical properties on Ag morphology. The inset of Figure 4 shows the electrode sheet resistance vs. the silver thickness for the different interlayers. The best electrical performance is obtained for the MoO_3 sample with the best wetting behavior. V_2O_5 shows the worst performance because the silver islands are not sufficiently connected, forming only worm-like structures. Without an interlayer, the electrode sheet resistance increases strongly with decreasing layer thickness. This hints at diffusion of silver into the organic layer forming a non-conductive mixed layer and unfavorable percolation behavior of the electrode layer. These results suggest the preferential usage of MoO_3 in an OSC as template for a thin silver electrode. Using MoO_3, the silver morphology is positively influenced, higher conductivity and partly improved transparency of the electrode are achieved, and the penetration of the noble metal into the organic layers is reduced. Thus more efficient solar cells are fabricated.

It is well known that transparent capping layers can increase the transmittance of a thin metal electrode leading to more efficient OSCs,[24,25] While the electrical performance of the electrode is not affected. In **Figure 5** the transmittance spectra of 11 nm thick Ag layers deposited on glass/BF-DPB (20 nm)/ MoO3 (4 nm) substrates are depicted. A capping layer of 50 nm tris-(8-hydroxy-quinolinato)-aluminum (Alq_3) increases

© 2012 WILEY-VCH Verlag GmbH & Co. KGaA, Weinheim

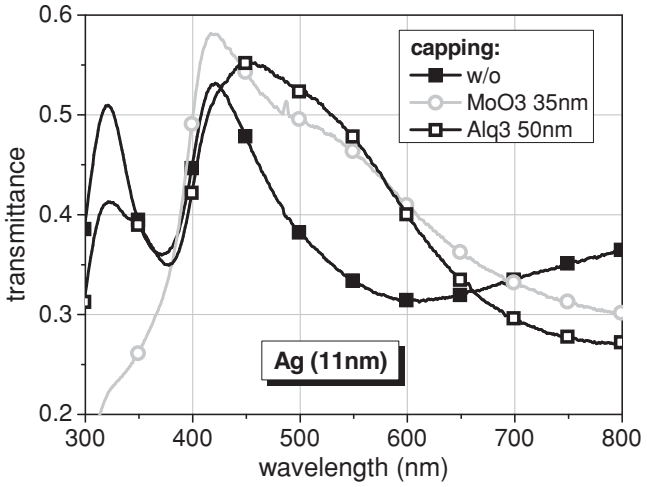

Figure 5. Transmittance of 11 nm Ag electrodes deposited on BF-DPB + 4 nm MoO_3 and glass substrate. The capping is varied with 35 nm MoO_3 (empty circles), 50 nm Alq_3 (open squares), or without (squares). Note that the MoO_3 capping cuts most of the UV light.

the transmittance over a broad spectral range. For instance at 500 nm the transmittance changes from 38% without the capping to 53% with Alq_3 capping. A similar increase is observed when 35 nm MoO_3 are applied. The major differences between the two capping layers are the organic/inorganic character, the refractive index and the transmission of UV light. As Alq_3 causes no significant absorption below 400 nm, the MoO_3 capping absorbs most of the UV light, as clearly seen in a sharp transmittance drop from 52% to 20% at 320 nm wavelength, which is beneficial for the UV sensitive organic materials used in OSCs.[26]

Figure 6 shows current-voltage curves of OSCs which use an 11 nm thin Ag layer as semitransparent top electrode and

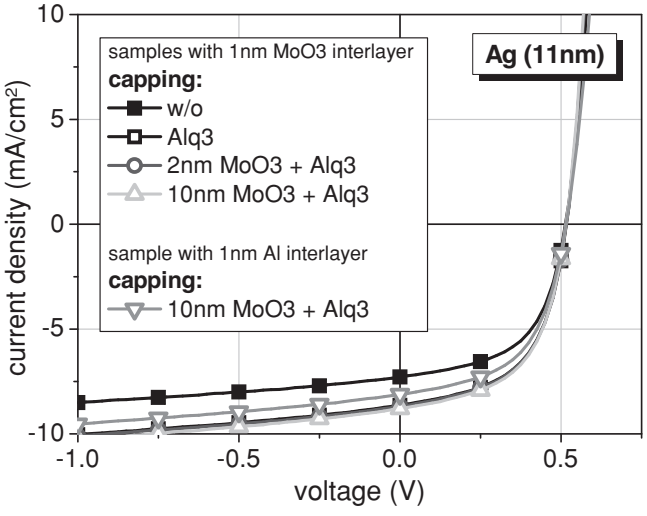

Figure 6. Current–voltage curves of OSCs with different capping layers, under illumination (100 mW/cm^2). The interlayer is varied with 1 nm MoO_3 or 1 nm Al to avoid intermixing of Ag and organic. The capping is varied with 50 nm Alq_3 (empty squares), 2 nm MoO_3 + 50 nm Alq_3 (empty circles), 10 nm MoO_3 + 50 nm Alq_3 (empty up triangles), or no capping (squares). The capping leads to improved photocurrent generation.

Table 2. Solar cell characteristics depending on the capping layer, obtained under illumination with 100 mW/cm^2. As an interlayer 1 nm MoO_3 or 1 nm Al is used respectively. For each material combination 4 identical samples are produced and efficiency deviations are stated.

capping	interlayer	V_{OC} [V]	J_{SC} [mA/cm^2]	*FF* [%]	η [%]
without	MoO_3	0.51	7.44	55.8	2.12 ± 0.01
50 nm Alq3	MoO_3	0.52	8.83	55.3	2.51 ± 0.01
2 nm MoO_3 + Alq_3	MoO_3	0.52	8.88	55.3	2.50 ± 0.03
10 nm MoO_3 + Alq_3	MoO_3	0.52	8.99	55.4	2.54 ± 0.04
10n m MoO_3 + Alq_3	Al	0.52	8.30	54.8	2.32 ± 0.02

a 50 nm Alq_3 capping for improved light incoupling. Additionally, 2 nm or 10 nm MoO_3 are deposited as interlayer directly on the thin silver electrode to study the influence of the inorganic surface passivation on device stability. On the bottom side of the thin silver electrode, the interlayer of 1 nm MoO_3 is also switched with a 1 nm aluminum (Al) interlayer to investigate passivation at the bottom interlayer. An aluminum interlayer is chosen because it hinders the interaction and interpenetration of silver and organic layers in the same way like MoO_3,[21] has been used as standard top-electrode in our institute before and yields a much better and fairer performance than without any interlayer. However, the difference between organic/metal and organic/oxide/metal interface is still given and apparently plays a major role for degradation. The corresponding solar cell characteristics are summarized in **Table 2**. The main influence of the capping is reflected in the short circuit current density. When the Alq_3 capping is applied, J_{SC} remarkably increases from 7.44 mA/cm^2 to 8.83 mA/cm^2 due to the improved light incoupling. It increases slightly further by using the additional thin MoO_3 layers. This can be explained by further optimization of the optical field in the device. Since open circuit voltage and fill factor remain almost constant at 0.52 V and 55%, respectively, an improved device efficiency of 2.6% is achieved. If aluminum is used as interlayer, the device efficiency drops to η = 2.3% due to the unfavorable metal morphology. It should be noted that with aluminum as interlayer an S-kink is not visible as it is observed for solar cells without bottom interlayer.

To investigate the stability of the ultra thin silver electrode we prepared similar OSCs as shown above but with a lower silver thickness of only 8 nm which is very close to the percolation threshold. At 8 nm the silver clusters are just connected which leads to higher sheet resistances, more plasmonic absorption and a drop in efficiency to 1.9%. However, for long-term measurements the 8 nm samples are preferred, because smallest changes in electrode performance are detectable, less interference with other device ageing effects is expected and the effect of MoO_3 is more pronounced. After encapsulation with a glass lid and a first characterization, the solar cells are transferred to a lifetime setup. It enables continuous illumination of the samples with white light of variable intensity, under controlled environmental conditions. We employ 45 ± 2 °C and a light intensity of 400 mW/cm^2 (4 suns) to achieve accelerated ageing,[27,28] measuring for more than 2200 h. **Figure 7** shows the device efficiencies of the samples changing over time, normalized to the first measurement point. The sample without MoO_3 capping

© 2012 WILEY-VCH Verlag GmbH & Co. KGaA, Weinheim

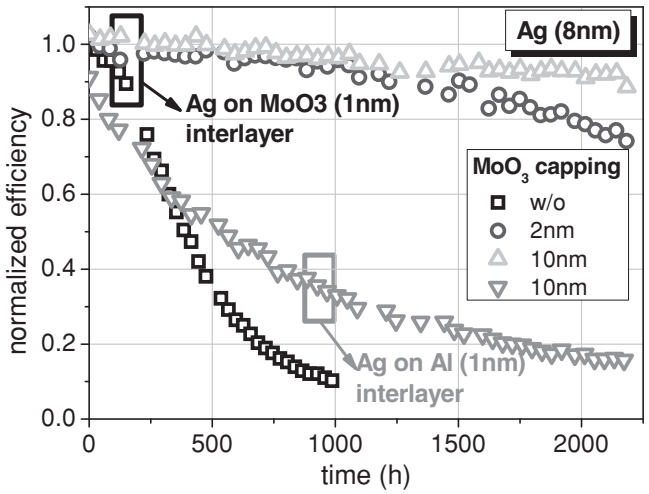

Figure 7. Time development of the normalized power conversion efficiency of OSC at an elevated light intensity of 4 suns (400 mW/cm^2). Device lifetime is increased with increasing capping layer thickness. Degradation occurs also on the interface between metal and organic layers which is reduced by 1 nm MoO_3 interlayer.

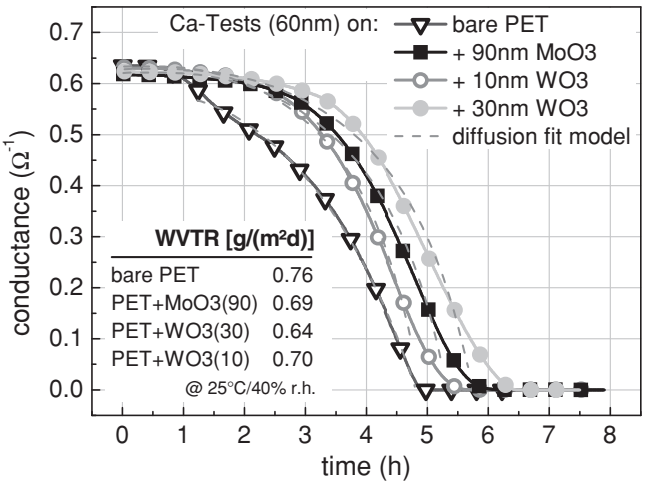

Figure 8. Permeation rate measurements on 125 µm thick PET (Melinex ST 504) films coated with 90 nm MoO_3 (squares), 10 nm WO_3 (empty circles), 30 nm WO_3 (circles), or uncoated PET (empty down triangles). As sensor a 60 nm thick calcium layer is used. A complex diffusion fit[30] is carried out to determine the WVTR.

layer degrades to 80% of the initial efficiency (T_{80}) already after 212 h, while its degradation is dominated by J_{SC} and *FF* (more information can be found in the Supporting Information Figure S3). For the samples with MoO_3 capping, a strongly increased OSC lifetime is observed. The sample employing a 10 nm thick MoO_3 capping enables a device lifetime (T_{80}) of approximately 4500 h (determined by linear fitting). This result is promising considering the accelerated degradation conditions. A similar but slightly lower improvement in lifetime is shown using a 2 nm thick MoO_3 capping. This indicates that the electrode stability is affected mostly by the interface between silver and top capping. To examine this effect for the bottom side of the silver electrode, we measured also the OSC with the 1 nm thick Al interlayer instead of the MoO_3 bottom interlayer. Again the device degradation is very fast (T_{80} = 86 h), showing that the interface between metal and organic layers is of high importance for a stable device. Thus, the metal thin film electrode can be greatly stabilized by introducing MoO_3 oxide layers at both interfaces.

Looking at the reasons for the fast degradation of the metal electrode, usually two major issues, oxidation or delamination exist.[29,13] Both are more pronounced the more oxygen or water is available to react with the electrode. To investigate whether the oxide offers a barrier against oxygen and water and thereby protection against both mechanisms, we deposited MoO_3 or WO_3 on PET (Melinex ST 504) films and measured their water vapor transmission rate (WVTR) via an electrical calcium tests, with the setup described elsewhere.[30] The results are depicted in **Figure 8**. The decrease in conductance of the calcium layer is closely related to the amount of water which passes through the coated PET. There is a little improvement of the barrier performance from 0.76 g/(m^{2}d) to 0.64 g/(m^{2}d) when employing oxides as additional barriers on PET. Also the lag time is enhanced from 1.3 h to ≈3 h. However, the barrier improvement is very small, even though the oxide layer thicknesses used in these experiments are much higher than in the OSC stack. Considering these results we can exclude the idea that the MoO_3 layers protect the silver electrode from oxygen and water. Another effect to take into consideration is the cut-off filtering of near-UV light by the oxide layers. However, while a reduction of UV light is certainly beneficial for the cell lifetime,[26] the degradation effect observed here is UV independent and can be related to the very thin and sensible silver electrode layer. This can be deduced from the lifetime data in Figure 7, since the UV filtering effect for the device with 10nm top-oxide and aluminum bottom-interlayer is equal or greater than for all other samples, but does not cause a longer device lifetime. The observed stabilization effect of the MoO_3 interlayers can be well explained by the interaction between metal and oxide which saturates the metal surface and passivates it against further reactions, thereby preventing metal delamination, diffusion and oxidation.

3. Conclusions

We have shown that thin silver layers thermally evaporated on different transition metal oxide interlayers (MoO_3, WO_3, and V_2O_5) are suitable as transparent top contact for organic solar cells. Due to a strong change in morphology the transmittance and conductance of the Ag layer is varied with the employed oxide interlayer. The oxide can also be employed as a top capping layer and improves the transmittance of the Ag electrode. The efficiency of an OSC test-device is increased from 1.5% without oxide layers to 2.6% using a 1 nm MoO_3 interlayer and a capping of 10 nm MoO_3 followed by 50 nm Alq_3. Additionally, it is shown that the ultrathin silver electrode is significantly stabilized when it is sandwiched between two MoO_3 layers, resulting in OSC lifetimes of T_{80} = 4500 h. We assume this stabilization is caused by the interaction between Ag and MoO_3 passivating the metal surface for further reactions. The effect of the MoO_3 layer, acting as an additional barrier against water

© 2012 WILEY-VCH Verlag GmbH & Co. KGaA, Weinheim

and oxygen permeation is excluded with electrical calcium test measurements.

4. Experimental Section

All samples shown in this publication were fabricated in a custom-made vacuum system (K.J. Lesker, UK) by thermal (co-)evaporation at a base pressure of 10^{-8} mbar, using shadow masks. As substrate Borofloat 33 glass (Schott, Germany; purchased from Prinz Optics, Germany) was used. It was carefully cleaned with acetone, ethanol, and oxygen plasma before being transferred into the vacuum chamber. During one processing run of 36 samples, the intentional variation of specific layers or parameters was possible for specific samples while all other layers were deposited under identical conditions. This allowed the inclusion of reference samples, which could be used for direct comparison within the run, and allowed for run to run comparisons for similar or equal stacks to validate processing over time. All layer thicknesses were monitored with calibrated quartz crystal monitors, in case of the very thin layers in the range of 1 nm, the layers were probably neither smooth nor closed, so the thickness given had to be interpreted as an equivalent thickness, indicating the amount of material on the sample. In this paper the metal, oxide interlayer and capping layer thicknesses were varied and their influence is investigated. The small molecule organic solar cells presented were n-i-p type, i.e., the intrinsic absorber (i) is embedded between dedicated electron (n) and hole (p) transport materials. The complete stack is shown in Figure 1. As cathode, 50 nm Ag were used. Its high reflectivity created a cavity in the device which enables improved light absorption. As the electron transport layer, 10 nm of C_{60} (BuckyUSA, USA; purified by CreaPhys GmbH, Germany) n-doped by $W_2(hpp)_4$ (Novaled AG, Germany) with 2 wt% were employed. 28 nm intrinsic C_{60} served as electron transport layer and acceptor followed by a bulk heterojunction consisting of C_{60} and zinc phthalocyanine (ZnPc, TCI EUROPE N.V., Belgium; purified by CreaPhys GmbH, Germany) (30 nm thickness) simultaneously evaporated with a weight ratio of 1:1. Next, 5 nm of intrinsic ZnPc were deposited. For efficient hole transport, 40 nm of *N,N′*((Diphenyl-N,N′-bis)9,9,-dimethyl-fluoren-2-yl)-benzidine (BF-DPB, Sensient AG, USA) doped with 10 wt% 2,2′-(perfluoronaphthalene-2,6-diylidene)dimalononitrile (F_6-TCNNQ, Novaled AG, Germany) were deposited. The following transient metal oxide interlayer was varied with molybdenum(VI) oxide (MoO_3), tungsten(VI) oxide (WO_3), vanadium(V) oxide (V_2O_5) (all from Sigma-Aldrich, USA, 99.99% purified) and compared to samples without an oxide interlayer. An ultrathin silver layer (8 nm–14 nm thickness) was used as an anode. For good charge carrier extraction, forming an ohmic contact, 1 nm of each pure dopant was deposited at the interfaces between both metal electrodes and the organic layers, respectively. Finally a capping layer of MoO_3 or/and tris-(8-hydroxy-quinolinato)-aluminum (Alq3) was deposited. All organic materials except the dopants were purified at least twice by vacuum gradient sublimation and were tracked in the material and processing database to ensure consistent material quality for all experiments. The completed solar cells were encapsulated with a transparent encapsulation glass, fixed by UV-hardened epoxy glue, in a nitrogen glovebox attached to the vacuum chamber. The photoactive active area of the OSC was 6.44 mm^2, as defined by the overlap of bottom and top electrode.

Current voltage measurements were carried out using a source measurement unit 2400 SMU (Keithley, USA) and simulated AM 1.5G sun light (16S-150 V.3 by Solar Light Co., USA) taking spectral mismatch into account. The illumination intensity was kept at (100 ± 1) mW/cm^2, monitored by a Si reference diode. All devices were exposed to similar aging conditions using a custom-made setup that was described previously.[27] For illumination, white LEDs with an emission spectrum in the range from 400 nm to 700 nm were used, set to an intensity leading to four times the J_{SC} under AM 1.5G (equivalent to 400 mW/cm^2, which simulates the radiation intensity of 4 suns).

Additional samples consisting of the top electrode only (transition metal oxide interlayer, silver electrode, capping) were fabricated and characterized by optical, electrical and morphological studies. Since the deposition of such thin layers was very substrate-dependent, the oxide interlayer and the silver were not only directly evaporated onto glass but on 20 nm p-doped BF-DPB. This was exactly the same layer below the electrode as was used in the OSC. Thus the growth of oxides and Ag was decoupled from the glass substrate and exhibited similar growth conditions as on top of the OSC. A four-point-probe measurement stand S 302-4 (LucasLabs, USA) was used to determine sheet resistances of the electrodes. SEM images were recorded using a Zeiss GSM 982 Gemini SEM. Several images were recorded at different positions to ensure reproducible results that actually represented the whole sample. The transmittance was measured using an Ava-Light-DH-S-Bal (Avantes BV, Netherlands) light source and a CAS 140 CT spectrometer (Instrument Systems GmbH, Germany) through an aperture of 2.96 mm^2. The preparation of the electrical calcium tests on glass substrates and their evaluation was described in a previous publication.[30] They were encapsulated with PET (Melinex ST 504) films, which were coated with oxide layers facing the calcium sensor.

Supporting Information

Supporting Information is available from the Wiley Online Library or from the author.

Acknowledgements

This work was funded by the German BMBF with support code 13N11060 (project acronym "R2Flex") and as part of the Dresdner Innovationszentrum für Energieeffizienz by the free state of Saxony, the European Union and the Fraunhofer Gesellschaft. The authors thank Susanne Goldberg from TU Dresden for the SEM measurements and Andreas Wendel and the rest of the Lesker-Team of IAPP, TU Dresden for sample preparation.

Received: June 13, 2012
Published online: July 25, 2012

[1] C. W. Tang, *Appl. Phy. Lett.* **1986**, *48*, 183.
[2] M. A. Green, K. Emery, Y. Hishikawa, W. Warta, E. D. Dunlop, *Prog. Photovoltaics* **2012**, *20*, 12.
[3] S. Reineke, F. Lindner, G. Schwartz, N. Seidler, K. Walzer, B. Luessem, K. Leo, *Nature* **2009**, *459*, 234.
[4] H. Klauk, *Chem. Soc. Rev.* **2010**, *39*, 2643.
[5] K. A. Sierros, N. J. Morris, K. Ramji, D. R. Cairns, *Thin Solid Films* **2009**, *517*, 2590.
[6] Y. H. Kim, C. Sachse, M. L. Machala, C. May, L. Müller-Meskamp, K. Leo, *Adv. Funct. Mater.* **2011**, *21*, 1076.
[7] J.-Y. Lee, S. T. Connor, Y. Cui, P. Peumans, *Nano Lett.* **2008**, *8*, 689.
[8] D. S. Hecht, L. Hu, G. Irvin, *Adv. Mater.* **2011**, *23*, 1482.
[9] M. Fahland, P. Karlsson, C. Charton, *Thin Solid Films* **2001**, *392*, 334.
[10] F. Li, S. Ruan, Y. Xu, F. Meng, J. Wang, W. Chen, L. Shen, *Sol. Energy Mater. Sol. Cells* **2011**, *95*, 877.
[11] D. W. Zhao, P. Liu, X. W. Sun, S. T. Tan, L. Ke, A. K. K. Kyaw, *Appl. Phys. Lett.* **2009**, *95*, 153304.
[12] R. Steim, F. R. Kogler, C. J. Brabec, *J. Mater. Chem.* **2010**, *20*, 2499.
[13] R. S. Sennett, G. D. Scott, *J. Opt. Soc. Am.* **1950**, *40*, 203.
[14] S. E. Roark, K. L. Rowlen, *Anal. Chem.* **1994**, *66*, 261.
[15] V. Zaporojtchenko, K. Behnke, A. Thran, T. Strunskus, F. Faupel, *Appl. Surf. Sci.* **1999**, *144*, 355.
[16] G. Rosenfeld, R. Servaty, C. Teichert, B. Poelsema, G. Comsa, *Phys. Rev. Lett.* **1993**, *71*, 895.

© 2012 WILEY-VCH Verlag GmbH & Co. KGaA, Weinheim

[17] M. Jørgensen, K. Norrman, F. C. Krebs, *Sol. Energy Mater. Sol. Cells* **2008**, *92*, 686.
[18] E. Voroshazi, B. Verreet, A. Buri, R. Müller, D. Di Nuzzo, Paul Heremans, *Org. Electron.* **2011**, *12*, 736.
[19] M. O. Reese, A. J. Morfa, M. S. White, N. Kopidakis, S. E. Shaheen, G. Rumbles, D. S. Ginley, *Sol. Energy Mater. Sol. Cells* **2008**, *92*, 746.
[20] W. Tress, K. Leo, M. Riede, *Adv. Funct. Mater.* **2011**, *21*, 2140.
[21] S. Olthof, J. Meiss, B. Lüssem, M.K. Riede, K. Leo, *Thin Solid Films* **2011**, *519*, 1872.
[22] J. R. Heath, *Phys. Rev. B* **1989**, *40*, 14.
[23] S.-K. Kim, H. S. Ee, W. Choi, S. H. Kwon, J. H. Kang, Y. H. Kim, H. Kwon, H. G. Park, *Appl. Phys. Lett.* **2011**, *98*, 011109.
[24] J. Meiss, M. Furno, S. Pfuetzner, K. Leo, M. Riede, *J. Appl. Phys.* **2010**, *107*, 053117.
[25] G. Leftheriotis, P. Yianoulis, D. Patrikios, *Thin Solid Films* **1997**, *306*, 92.
[26] M. Hermenau, M. Riede, K. Leo, *Degradation of Small Molecule Based OPV. Stability and Degradation of Organic and Polymer Solar Cells*, John Wiley & Sons Inc., Weinheim **2012**, p. 132.
[27] M. Hermenau, K. Leo, M. Riede, *Proc. SPIE* **2010**, *7722*, 77220K.
[28] M. Hermenau, S. Scholz, K. Leo, M. Riede, *Sol. Energy Mater. Sol. Cells* **2011**, *95*, 1278.
[29] M. Hermenau, S. Schubert, H. Klumbies, J. Fahlteich, L. Müller-Meskamp, K. Leo, M. Riede, *Sol. Energy Mater. Sol. Cells* **2012**, *97*, 102.
[30] S. Schubert, H. Klumbies, L. Müller-Meskamp, K. Leo, *Rev. Sci. Instrum.* **2011**, *82*, 094101.

© 2012 WILEY-VCH Verlag GmbH & Co. KGaA, Weinheim